ACS Sustainable Chemistry & Engineering

pubs.acs.org/journal/ascecg

Research Article

Copper 3D-Printed Electrodes for Ammonia Electrosynthesis via Nitrate Reduction

Juan V. Perales-Rondon, Daniel Rojas, Wanli Gao, and Martin Pumera*

Cite This: *ACS Sustainable Chem. Eng.* 2023, 11, 6923−6931

Read Online

ACCESS | Metrics & More | Article Recommendations | Supporting Information

ABSTRACT: Ammonia is critical to the world economy. However, nowadays the production of ammonia is exclusively carried out by the well-known Haber−Bosch process, which is an energy-intensive process that leads to a large amount of CO_2 emissions. The search for alternative ammonia production routes is mandatory for a sustainable and zero emissions future economy. Electrochemical nitrate-to-ammonia conversion emerges as a suitable alternative to achieve decentralized ammonia production at a small scale with zero emissions perspective. Here, we fabricate copper electrodes by a three-dimensional (3D) printing technique, which allows for the point-of-use customizable fabrication of electrochemical systems, and use them for nitrate-to-ammonia conversion. By using the fused fabrication filament printing technique, Cu-based electrodes were prepared in an easy, fast, and scalable way from a Cu-containing filament. The electrode was used for nitrate-to-ammonia conversion, obtaining an outstanding faradaic efficiency (FE) of 96.5% and a high ammonia selectivity of 95%. The fabrication of a copper-based electrochemical system for nitrate-to-ammonia conversion paves the way for an on-demand, point-of-use scalable electrochemical system for ammonia production.

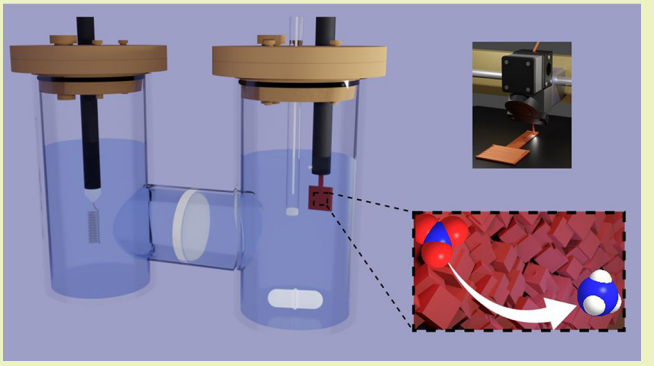

KEYWORDS: *ammonia synthesis, Cu electrodes, 3D printing, nitrate reduction, nanostructuring*

INTRODUCTION

Ammonia is a fundamental molecule not only for sustaining life but also for industrial and energy-related applications.[1−3] The annual production of ammonia was 175 million metric tons (Mmt) in 2019, and this value is increasing year by year, placing ammonia as one of the largest human-synthesized chemicals.[4] This points out the importance of ammonia for the global economy and development.[5] Most of the ammonia is produced by the well-known Haber−Bosch (H−B) process based on the combination of H_2 and N_2 at high pressure (100 atm) and high temperature (700 K). These specific requirements make the H−B process an energy-intensive industrial process, consuming around 2% of the worldwide energy output. In addition, most of the H_2 employed in the H−B process comes from the steam methane reforming and water−gas shift reaction, with consequent greenhouse gas emission in the form of CO_2.[6] Therefore, alternative ways of producing ammonia with less environmental impact are urgently needed.

Among the different techniques to produce ammonia, the electrochemical methods emerge as promising approaches, with electrochemical reduction of nitrogen being the most widespread method.[7,8] However, its development has been tarnished by the low yielding rate, with no practical applications so far.[9] In this sense, electrochemical nitrate-to-ammonia conversion emerges as an ideal alternative to replace the H−B process to produce ammonia at a small and decentralized scale.[10] Moreover, the use of electrochemistry can take advantage of the renewable energy supply, it is compatible with the construction of full compact devices (electrolyzers) and could be integrated with on-flow water treatment,[10] which enhances the interest in its development. The electrochemical nitrate reduction to ammonia (NRA) reaction is complex, with two main challenges to be faced: on the one hand, the large number of intermediate products that are thermodynamically expected in the desired potential window, and on the other hand, the use of high overpotentials, which brings hydrogen evolution as a competing reaction for active sites. To address these two main challenges, the understanding of the electrochemical NRA at a fundamental level is mandatory, providing the guidelines for the efficient electrocatalyst design. Since nitrate reduction is a surface-sensitive reaction, suitable electrocatalysts with a compromise between H adsorption and NO_3^- adsorption capabilities are

Received: November 15, 2022
Revised: April 9, 2023
Published: April 25, 2023

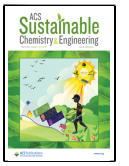

https://doi.org/10.1021/acssuschemeng.2c06851
ACS Sustainable Chem. Eng. 2023, 11, 6923−6931

desirable. To achieve a better performance of the electrocatalyst, a careful control of the structure and composition of the electrode surface is critical. By using surface engineering, both the surface composition and structure of the electrode can be tailored to improve the efficiency and stability of the electrocatalyst. One of the state-of-the-art electrocatalysts for ammonia synthesis from nitrate is the CuO/Cu_2O material,[11,12] which has shown a high faradaic efficiency (FE) up to 95% and high ammonia selectivity (81%) at −0.80 V vs reversible hydrogen electrode (RHE). A recent study has shown that the origin of the high activity and stability of an electrocatalyst depends on the composition of the oxide material, being responsible for the activity the Cu/Cu_2O structure resulting from the electrochemical conversion of CuO at a lower potential in the electrolytic medium.[13] On the other hand, some previous works have also stressed the role of the surface structure of the electrocatalyst in the enhancement of the FE and selectivity, stating that {100} facets are more active for nitrate reduction with a high selectivity in ammonia production.[14]

In recent years, fused fabrication filament (FFF) three-dimensional (3D) printing, also known as fused deposition modeling (FDM), has attracted great interest due to the capabilities of rapid prototyping, scalability, and decentralization of the fabrication of objects with high customizability.[15,16] In the electrochemistry field, FFF-printed electrodes have been traditionally fabricated using conductive filaments composed of an insulating thermoplastic matrix (poly(lactic acid) (PLA) or acrylonitrile butadiene styrene (ABS)) and a carbon-based conductive filler. Nevertheless, these printed electrodes require aggressive and time-consuming postprinting activation protocols, using toxic organic solvents and/or high voltages to achieve electrochemically active electrodes.[17,18] In order to create 3D-printed metallic electrodes that can overcome these drawbacks, selective laser melting (SLM) was commonly used. However, the equipment is highly expensive and requires trained personnel in contrast to the very simple and widespread FFF.[19,20] In this regard, it has been recently demonstrated that FFF-printed electrodes can be fabricated using copper/PLA filaments after a simple sintering process, which is paving the way for new applications in electrosynthesis and energy conversion and storage.[21]

Herein, we report the preparation and modification of Cu-based 3D-printed electrodes for efficient ammonia synthesis from nitrate. The 3D-printed electrodes were sintered and nanostructured using an electrochemical method, followed by a chemical treatment to produce a faceted surface. The electrodes have shown to be highly efficient for ammonia synthesis with an outstanding FE at −0.92 V. This is the first time that a Cu-based 3D-printed electrode is used for NRA, which opens new avenues into the development of future scalable electrode materials for NRA.

MATERIALS AND METHODS

Reagents and Materials. All chemical agents were purchased from Merck and Sigma-Aldrich Co., Ltd., which included potassium nitrate (KNO_3), potassium hydroxide (KOH), hydrochloric acid (HCl), sulfamic acid (H_3NSO_3), *p*-aminobenzenesulfonamide ($H_2NC_6H_4SO_2NH_2$), *N*-(1-naphthyl) ethylenediamine dihydrochloride ($C_{10}H_7NHCH_2CH_2NH_2{\cdot}2HCl$), phosphoric acid ($H_3PO_4$), sodium hydroxide (NaOH), citric acid ($C_6H_8O_7$), salicylic acid (2-(HO)$C_6H_4CO_2H$), sodium hypochlorite solution 6−14% (NaClO), sodium nitroferricyanide ($Na_2[Fe(CN)_5NO]$), ammonium chloride (NH_4Cl), and sodium nitrite ($NaNO_2$). All solutions were prepared using ultrapure water obtained from a Millipore DirectQ purification system provided by Millipore (18.2 MΩ cm resistivity at 25 °C).

Cu-Based 3D-Printed Electrode Preparation. 3D printing of the Cu-based electrodes was done by FFF using Cu/PLA filament (The Virtual Foundry) in a Prusa i3 MK3S printer (Prusa Research) with a brass nozzle with a diameter of 0.6 mm (T_{nozzle} = 230 °C, T_{bed} = 60 °C). The design was created using Autodesk Fusion 360 software and the G-code was created using the Prusa Slicer software considering 100% infill and 0.1 mm layer height. The electrode design was composed of a 10 × 10 mm square connected to a 20 × 2 mm rectangle which acts as an electrical connector. In order to obtain electrically conductive electrodes, a thermal treatment needs to be performed to remove the PLA and sinter the metallic copper microparticles. To do so, electrodes were placed in a ceramic crucible (The Virtual Foundry) which is filled with Al_2O_3 as a refractory material. The crucible containing the electrode and refractory material is covered with a layer of sintering coconut charcoal (The Virtual Foundry) in order to create an inert atmosphere inside the furnace due to the reaction between carbon and oxygen at the high temperatures reached during the sintering, avoiding the oxidation of Cu, which will prevent the sintering process. The crucible is then placed inside the furnace and is heated up with the following temperature ramp: 0−300 °C at 5 °C min^{-1}, 300−1010 °C at 3 °C min^{-1}, and 1010−1060 °C at 1 °C min^{-1}. Finally, 1060 °C is held for 60 min and the oven is allowed to cool down to room temperature. After the sintering process, the electrodes were activated by immersion in 1 M HNO_3 for 15 min under bath sonication.

Characterization. The scanning electron microscopy (SEM) and energy-dispersive X-ray spectroscopy (EDS) images were obtained with a MIRA 3 SEM (TESCAN) and a Bruker XFlash 5010 EDS with an accelerating voltage of 20 kV. Alternatively, some SEM images were taken with a Verios 460L (Thermo Fisher Scientific (TFS)) with an electron beam accelerating voltage of 5 kV. The X-ray diffraction (XRD) was recorded with an X-ray powder diffractometer Rigaku SmartLab 3kW, using Cu Kα radiation (λ = 0.154 nm) operated at a current of 30 mA and a voltage of 40 kV. X-ray photoelectron spectroscopy (XPS) was measured using an AXIS Supra instrument from Kratos Analytical (Manchester, U.K.) with monochromatized Al Kα excitation (1486.7 eV) with a pass energy of 80 and 20 eV for the acquisition of the survey and high-resolution spectra, respectively. The binding energies were calibrated to the C 1s peak at 284.8 eV. The ultraviolet−visible (UV−vis) absorbance spectra were measured on a double-beam Jasco Co. Model V-750 with a wavelength range of 190−900 nm.

Electrochemical Measurements. The electrochemical measurements were carried out using an Autolab PGSTAT204 (Metrohm), in an H-type electrolytic cell with a frit separation. The Cu-based 3D-printed electrode, a commercial Ag/AgCl, and a platinum wire were used as the working, reference, and counter electrodes, respectively. The surface area of the working electrode was controlled by the initial 3D-printed design. On average, the total area exposed in each experiment using the sintered electrodes was 1.51 ± 0.09 cm^2. 1 M KOH solution + 0.1 M KNO_3 (80 mL) was added to the cathode and anode compartment. All potentials were recorded against the reversible hydrogen electrode (RHE). The electrolytic experiments were carried out at different potentials ranging from −0.42 to −1.22 V vs RHE for 1 h under constant magnetic stirring.

Electrochemical active surface area (ECSA) values were also calculated by using the double layer capacitance method. This method consists of performing different voltammetric experiments varying the scan rate of the cyclic voltammetry, i.e., 0.020, 0.040, 0.060, 0.080, 0.10, 0.12, 0.14, 0.16, 0.18, and 0.20 V s^{-1}. After performing the voltammetric experiments, the current density is measured at a fixed potential, that coincides with the middle potential in the cyclic voltammetry either in the positive or negative sweep. Those values are plotted against the scan rate, and the slope of the curve is the double layer capacitance (C_{dl}). The ECSA value is calculated by using eq 1

$$A = \frac{C_{dl}}{C_s} \tag{1}$$

https://doi.org/10.1021/acssuschemeng.2c06851
ACS Sustainable Chem. Eng. 2023, 11, 6923−6931

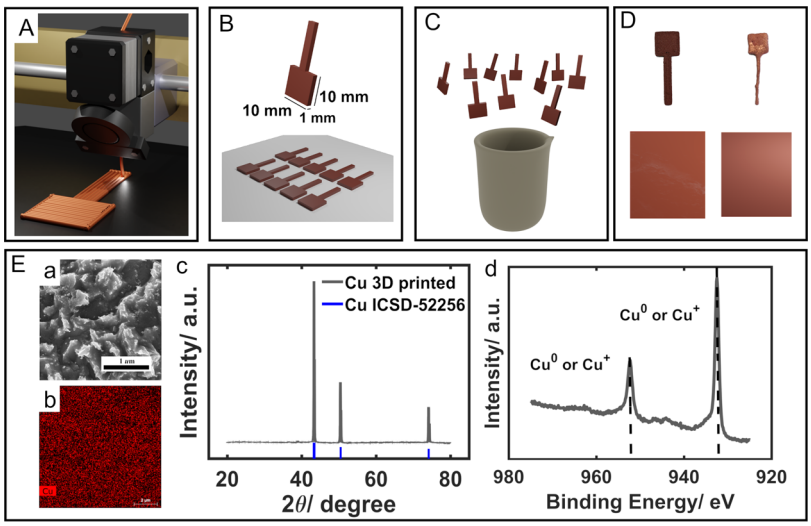

Figure 1. Schematic of the preparation of the 3D-printed electrodes. (A) Schematic representation of the 3D printer by FDM technology. (B) The printing process, from the electrode design to the printing as well as the dimensions of the electrodes. (C) Sintering of the electrodes by using a temperature program in a high-temperature oven. (D) Photography and representative model of the surface of the electrodes just printed (left) and after immersion in 1 M HNO_3 solution (right). (E) Characterization of the electrode after sintering and cleaning in 1 M HNO_3 solution: (a) SEM image, (b) EDX mapping, (c) XRD pattern, and (d) XPS analysis.

where A is the area in cm^2 and C_s is the specific capacitance. For a flat Cu surface, the value for C_s ranges between 20 and 60, 40 $\mu F\ cm^{-2}$ being the value selected for the calculation along this work.[13]

Colorimetric Determination of Ion Concentrations. Well-known colorimetric methods were used to determine the ion concentration of different products after performing the electrolytic experiments. An ultraviolet−visible (UV−vis) spectrophotometer was used to detect the concentration of different reagents/products of pre- and post-test electrolytes after an appropriate dilution to match the concentration range of calibration curves.

Determination of Ammonia. As a first step, an aliquot of electrolyte was taken out from the electrolytic cell and diluted to the desired detection range until 600 μL of solution. After that, 600 μL of a 3 M NaOH solution containing 10 wt % salicylic acid and 10 wt % sodium citrate was added to the solution, followed by the addition of 300 μL of 0.20 M NaClO and 60 μL of 2.0 wt % $C_5FeN_6Na_2O$ (sodium nitroferricyanide) solution. The resulting solution was allowed to rest for 2 h, after which the UV−vis absorption spectrum was taken. The formation of the indophenol blue product was determined using the absorbance at a wavelength of 655 nm.[13] The calibration curve was obtained by using standard solutions of ammonium chloride.

Determination of Nitrate. In a first step, an aliquot of electrolyte was taken out of the electrolytic cell and diluted to 5 mL to the detection range. Then, 0.1 mL of 1 M HCl and 0.01 mL of 0.8 wt % sulfamic acid solution were added to the initial dilution. The absorption spectrum was measured using an UV−vis spectrophotometer, and the absorption intensities at a wavelength of 220 and 275 nm were recorded. According to the reported method,[22] the final absorbance value was calculated by the equation Abs = Abs(220 nm) − 2Abs(275 nm). The calibration curve was performed by using a series of standard potassium nitrate solutions.

Determination of Nitrite. To carry out nitrite determination, a previously reported protocol was used.[22,23] Briefly, the color reagent was prepared by adding *p*-aminobenzenesulfonamide (0.4 g), *N*-(1-naphthyl) ethylenediamine dihydrochloride (0.02 g), ultrapure water (5 mL), and phosphoric acid (1 mL, ρ = 1.70 g mL^{-1}). An aliquot of electrolyte was taken out from the electrolytic cell and diluted to 1.5 mL to the detection range. Next, 50 μL of color reagent was added into the aforementioned 1.5 mL solution, followed by the addition of 100 μL of phosphoric acid (ρ = 1.70 g mL^{-1}) and evenly mixed. Finally, the absorption intensity at a wavelength of 540 nm was recorded after resting for 20 min. The concentration−absorbance curve was calibrated using a series of standard sodium nitrite solutions.

Determination of Ammonia by the ^{1}H NMR Quantitative Method and Isotopic Labeling Experiment. After electroreduction, the electrolyte was taken out from the cell. 250 μL of concentrated H_2SO_4 was added to 5 mL of electrolyte to adjust the pH value to be acidic for quantification by ^{1}H NMR (500 MHz) with internal standards of maleic acid. The calibration curve was created as follows: first, a series of known concentrations of $^{14}NH_4^+$ (50, 100, 150, 200, 250 ppm) were prepared in 1 M KOH + 0.1 M KNO_3 as standards; second, 5 mL of the standard solution with different concentrations was mixed with 0.002 g of maleic acid. After that and before measuring, 500 μL of this solution was placed in an NMR tube and 50 μL deuterium oxide (D_2O) was added for the NMR detection. The calibration curve was achieved using the peak area ratio between $^{14}NH_4^+$ and maleic acid.

For the isotopic labeling experiment, an electrolytic experiment was carried out with an initial concentration of $K^{15}NO_3$. After the electrolysis, the electrolyte was taken out from the cell, and a similar procedure as that performed for the calibration curve was developed. The corresponding doublet signal of $^{15}NH_4^+$ was obtained in the ^{1}H NMR experiment.

Calculation of Different Parameters to Evaluate the Performance of the Electrocatalyst.

$$FE_{NH_3} = \frac{8Fn_{NH_3}}{Q} \times 100\% \quad (2)$$

$$\text{selectivity} = \frac{n}{\Delta n_{NO_3^-}} \times 100\% \quad (3)$$

$$\text{yield rate (YR)} = \frac{n_{NH_3}}{tA} \quad (4)$$

where F is the faradaic constant (96 485 C mol^{-1}), n_{NH_3} is the number of mol of NH_3 calculated from the corresponding colorimetric method, n is either the number of moles of NH_3 or NO_2^- calculated from colorimetric methods, $\Delta n_{NO_3^-}$ is the mol difference of NO_3^- before and after electrolysis, n_0 is the initial concentration of NO_3^-, t is the electrolysis time (1 h), A is the area of the electrode, and Q is the total charge passing through out the electrode during the electrolytic experiment.

https://doi.org/10.1021/acssuschemeng.2c06851
ACS Sustainable Chem. Eng. 2023, 11, 6923−6931

RESULTS AND DISCUSSION

Preparation and Activation of Cu-Based 3D-Printed Electrodes. Figure 1 presents a schematic of the electrode preparation by a 3D-printed procedure. Initially, a Cu-based filament was used to prepare the Cu 3D-printed electrodes. In a typical procedure, the electrodes are printed out using the FFF technique (Figure 1A) in a squared form (1 cm^2 area) with a rectangular extension to allow an electrical connection (Figure 1B). After being printed, the electrodes need to be turned electrically conductive by eliminating PLA and sintering the Cu particles contained in the filament (Figure 1C). Figure 1D shows a model of the surface, as well as a picture about the change on the electrode before (left) and after (right) sintering. It is worth noting that without sintering, the conductivity and metal character of the electrodes is negligible. After sintering and dipping in 1 M HNO_3 solution for 15 min under bath sonication, the electrode presents a cuprous bright color, which suggests the formation of a metallic phase on the electrode surface (Figure 1D right). It is important to notice that after the sintering, the electrode is covered by alumina particles that were used in the sintering process. However, after sonication in nitric acid, these particles, which are only attached to the electrode surface, are removed, leaving the surface clean to be used. The structure and composition of the resulting electrode are given in Figure 1E. The SEM image shows a rough surface, which is expected since the treatment in nitric acid promotes a chemical etching of the as-prepared electrode. Furthermore, energy dispersive X-ray spectroscopy (EDX) mapping demonstrates that Cu is the main component of the electrode. The XRD pattern shows typical peaks of Cu cubic (ICSD-52256), with three main characteristic peaks at 43.3, 50.4, and 74.1°. Additionally, high-resolution Cu 2p XPS analysis shows two main peaks at 932.5 and 952.3 eV corresponding to the presence of Cu^0, which agrees with obtaining a solid copper electrode. The XPS survey for the same sample is shown in Figure S1 in the Supporting Information. Finally, no presence of Al/Al_2O_3 is detected after the cleaning process (HNO_3 1 M) as shown in the XPS survey spectrum, which ensures that no other material is interfering in the catalytic activity of the as-prepared 3D-printed electrodes.

Nanostructuring of the Cu-Based 3D-Printed Electrodes. After activating the electrodes in 1 M HNO_3 solution, an electrochemical modification (KCl-treated) followed by a chemical treatment ($NaHCO_3$-treated) was used to promote the nanostructuring of the electrode surface. In the first stage, electrochemical oxidation of the Cu electrode was carried out by using amperometric oxidation at +1.10 V vs Ag/AgCl for 100 s in 0.1 M KCl.[24] Figure 2A depicts the models and images of the electrode after each treatment, whereas Figure 2B depicts the SEM images and EDX mapping for the electrode after the KCl treatment (Figure 2B(a–c)). Well-defined nanocubes on the electrode surface are formed after the electrochemical oxidation. This result agrees with the literature,[25,26] where the oxidation–reduction cycles of a Cu electrode promote the electrochemical generation of nanocubes, particularly under Cl^- containing electrolytes. A high density of nanocubes of ca. 200 nm side with a good monodispersion (Figure S2) were found on the electrode treated with the amperometric protocol. It has been reported that in these electrolytic conditions, the oxidation of a Cu electrode promotes the formation of CuCl nanocubes.[24,27]

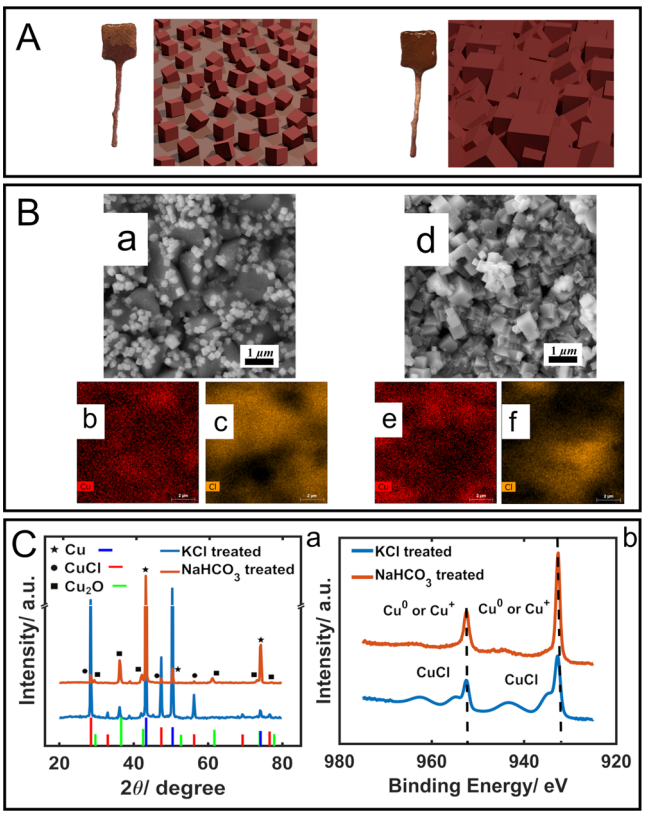

Figure 2. Characterization of treated Cu-based 3D-printed electrodes. (A) The real photograph and representative model of the surface of the electrodes: KCl-treated (left) and $NaHCO_3$-treated (right). (B) SEM images and EDX mapping of the electrodes: (a–c) KCl-treated and (d–f) $NaHCO_3$-treated. (C) (a) Comparison of the normalized XRD spectra taken for the two treated electrodes and (b) comparison of the high-resolution Cu 2p XPS detailed spectra for the two treated electrodes.

EDX analysis shows a major composition of Cu and Cl, which is expected due to the oxidation of the electrolytic media. This was also confirmed by calculating the composition of the electrode surface by XPS data (Table S1). XRD analysis for the KCl-treated electrode (Figure 2C) shows the characteristic pattern of CuCl cubic compound with more prominent peaks at 28.5, 47.4, and 56.2, which correspond to Nantokite (ICDS-73255), marked with a circle symbol. This is further demonstrated by analyzing the high-resolution Cu 2p XPS spectrum, where peaks of Cu^+ are present (932.7 and 952.5 eV). Additionally, a peak corresponding to Cl^- is found at 198.8 and 269.8 eV in the survey XPS spectrum (Figure S3A). The freshly electrochemically treated electrode was subsequently immersed for 10 min in a solution containing 0.10 M $NaHCO_3$ to further promote nanostructuring of the surface.[24] Figure 2B(d–f) shows a SEM image and the corresponding EDX analysis of the electrode after chemical treatment. Additionally, the XRD pattern mainly corresponds to Cu_2O (ICDS-53322), with characteristic peaks at 36.59, 42.5, 61.7, and 73.9 marked with a square symbol. XPS analysis also confirms the presence of Cu_2O in the Cu 2p high-resolution spectrum (XPS survey found in Figure S3B), where, again, peaks centered at 932.7 and 952.5 eV, corresponding to Cu^+ are found. This is consistent with the formation of Cu_2O compound on the electrode surface. Additionally, the character of Cu^+ observed by the high-resolution Cu 2p spectrum could

https://doi.org/10.1021/acssuschemeng.2c06851
ACS Sustainable Chem. Eng. 2023, 11, 6923–6931

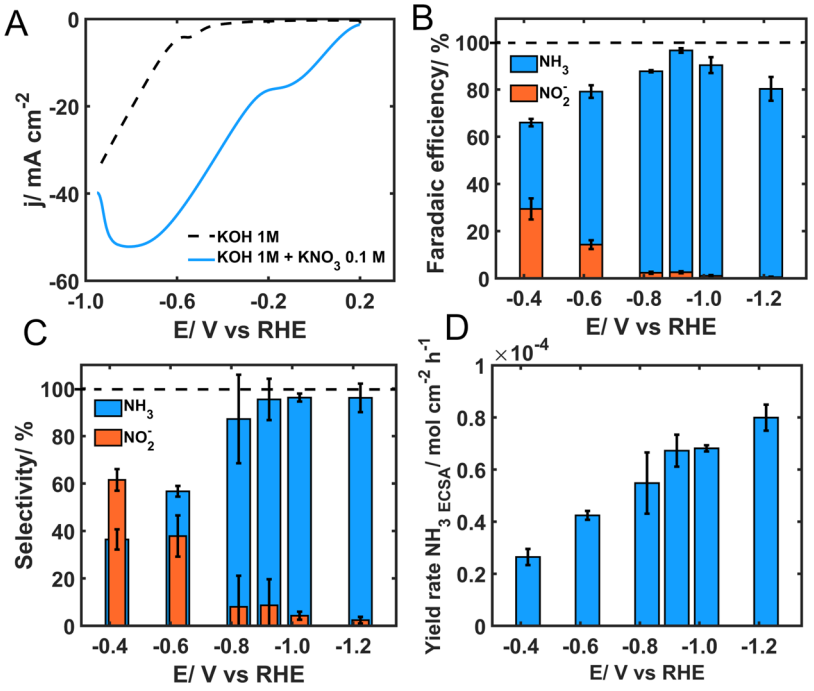

Figure 3. (A) LSV for $NaHCO_3$-treated Cu 3D-printed electrode in KOH 1 M with and without KNO_3 0.1 M. (B) FE for NH_3 and NO_2^- on electrolytic experiments at different potentials. (C) Selectivity of NH_3 and NO_2^- at different potentials. (D) Potential-dependent YR for NH_3 production. All of the electrolytic experiments were performed with a $NaHCO_3$-treated Cu 3D-printed electrode.

be also confirmed by the signal of the high-resolution Cu LMM region, where a peak centered at 570.1 eV is found (Figure S4). Interestingly, the number of cubic facets highly increases after immersion of the electrode in the solution. Moreover, the density of facets {100} exposure has a dramatic increase after the treatment. Finally, facets of cubes experience a growth in size compared to those resulting from the electrochemical treatment, suggesting a net increase in the surface area. It is worth noting that the $NaHCO_3$ solution has an alkaline character (pH 9). As has been suggested,[24] under these conditions, CuCl is less stable and decomposes to form the corresponding oxide-forming reaction that converts the CuCl into Cu_2O on the electrode surface, which explains the spectacular morphological change and the increase in the {100} facet density on the surface of the electrode. It is noteworthy that from the composition calculated by using XPS data (Table S2), the Cl content has been reduced considerably compared with the KCl-treated sample, which further confirms the effectiveness of $NaHCO_3$ treatment to convert CuCl into copper oxide-based electrodes. Therefore, a very well nanostructured electrode has been easily formed under this treatment protocol with a preferential formation of cubic nanostructures of the Cu_2O composition. This easy-to-implement treatment is perfectly compatible with the Cu 3D-printed electrodes, providing a fast and cost-effective strategy to modify electrodes of different morphologies in an active and desired nanostructuring. This could also be used when scaling up electrode modification protocols for other uses as electrocatalytic material.

Electrochemical Nitrate Reduction to Ammonia. 3D-printed electrodes modified by the electrochemical/chemical treatment were used to carry out NRA. The electrochemical NRA was carried out versus an Ag/AgCl reference electrode in 1 M KOH containing 0.1 M KNO_3. Every electrochemical experiment was recorded with a freshly prepared electrode after nanostructuring. First, linear sweep voltammetry (LSV) of the electrode were recorded in the presence and absence of NO_3^- (Figure 3A). As can be clearly seen, in the presence of NO_3^- (blue curve), current density starts to increase at a lower potential compared with the LSV in KOH, which is a clear indication that the electrode is active for the NRA reaction in such conditions. A voltammetric curve expressed in terms of ECSA is shown in Figure S5a, where still a reasonably high current density is observed for the reduction process. Two different reduction bands can be observed in the LSV (blue curve), the first one located at around −0.20 V and the other one peaking around −0.80 V. For the first region (around −0.2 V), no obvious cathodic signal is registered in the blank, out of the mostly capacitive current. Therefore, this peak should be related with some intermediate from the NO_3^- reduction process. Some previous works in the literature have reported nitrite reduction around this potential region for copper oxide-based electrodes,[28] which might suggest that the main product at these potentials is nitrite. To further demonstrate this point, an electrolytic experiment at potential −0.12 V vs RHE was carried out, with the consequent quantification of the amount of nitrite afterward (Figure S5b). As expected, the FE for nitrite in this experiment was in the amount of 75%, which indicates that this peak at −0.20 V is mainly due to nitrite formation. For the second region, a broad peak around −0.80 V was observed, which might be mostly associated to the complete reduction of nitrate into ammonia; however, more electrolytic experiments should be carried out to confirm this. It is noteworthy that in this first peak, no obvious bubble production was observed during the voltammetric experiment, while at potentials more negative than the second peak (from −0.90 V), some bubbles generation was observed. This suggests that at potentials more negative than −0.90 V, the HER could be taking place, becoming a dominating reaction over NRA on the electrode surface at more cathodic potentials.

https://doi.org/10.1021/acssuschemeng.2c06851
ACS Sustainable Chem. Eng. 2023, 11, 6923−6931

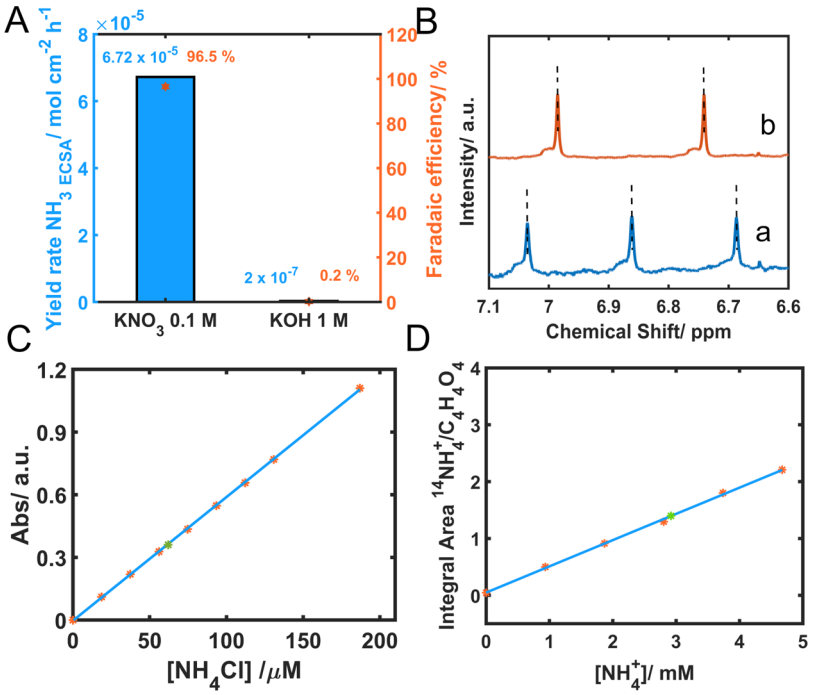

Figure 4. (A) YR and ammonia FE obtained after 1 h of electrolysis of a solution containing only KOH 1 M and KOH 1 M + KNO_3 0.1 M over a Cu-based 3D-printed electrode after $NaHCO_3$ treatment at −0.92 V. (B) ^1H NMR spectra of the electrolyte after electrocatalytic nitrate-to-ammonia conversion at −0.64 V, using $K^{14}NO_3$ (a) and $K^{15}NO_3$ (b) as the nitrogen source. (C) Calibration curve for ammonia determination using the colorimetric indophenol blue method. (D) Calibration curve for ammonia determination using the ^1H NMR method. In both calibration curves, the measured sample is marked as a star.

This fact can be also inferred from the LSV for the blank (black dashed curve), where the current density of the electrode at this cathodic region increases considerably, and clear bubble generation is observed in KOH 1 M.

After testing the electrode by using LSV, NRA was carried out by performing electrolytic experiments at different potentials to determine the efficiency of the electrode for ammonia production. The reactant and reductive products were measured using standard colorimetric methods as described in the experimental section. Calibration curves with the analytical range and the typical signal for each colorimetric method are given in Figures S6−S8. After performing electrolytic experiments, $NaHCO_3$-treated Cu 3D-printed electrode showed a volcano-shaped curve in FE, with a maximum of 96.5% at −0.92 V (Figure 3B) in agreement with some works in the literature,[13] which report the maximum for FE in copper-based electrodes around −0.85 and −0.90 V.

Moreover, ammonia selectivity gradually increases reaching a value of 95.6% at −0.92 V. At the following potentials, selectivity achieves a stable value (around 95−96%) from −0.92 V onward, while nitrite selectivity gradually declines, going from around 61% at −0.42 V to less than 3% at the following potentials. Comparative FE results for the three electrodes studied over the entire potential region are shown in Figure S9, where similar trends are observed for all three electrodes (maximum FE at −0.92 V). Even so, $NaHCO_3$-treated Cu 3D-printed electrode still exhibits the highest values of FE at the entire potential region. Ammonia YR normalized by the ECSA after electrolysis shows the highest value at −1.22 V; however, at −0.92 V, YR has a significantly high value (6.72×10^{-5} mol cm^{-2} h^{-1}) to be considered as an operating potential for a future application in electrolyzers. YR values were also calculated considering ECSA before and after electrolysis, and comparison results are shown in Figure S10. Examples of the ECSA calculation for the $NaHCO_3$-treated Cu 3D electrode are shown in Figure S11. There is a big change depending on the ECSA that is considered to calculate the YR value. In fact, considering ECSA values before electrolysis (Table S3), the Cu 3D electrodes are more active in terms of YR due to the lower area before electrolysis. It is well-known that copper-based electrodes undergo a considerable transformation during electrolytic experiments,[25,29] and such changes can lead to a variation in the ECSA. Indeed, a huge change in ECSA is clearly observed in the reported values in Table S3. Therefore, the YR was calculated with the ECSA after electrolysis since this value better shows the real performance of the electrode.

In the electrochemical synthesis of ammonia, demonstrating that the nitrogen source of the ammonia comes from nitrate in the solution and not from any other source is critical. To exclude any interference from the external environment, a blank solution was tested in the same conditions. Figure 4A shows FE and YR for two different solutions, one containing only the electrolyte (KOH 1 M) and the other with the addition of KNO_3 0.1 M. As can be observed, ammonia is produced exclusively from nitrate in solution, and negligible ammonia yield (2×10^{-7} mol cm^{-2} h^{-1}) is found in the solution containing only the electrolyte. An isotopic labeling experiment was also conducted using $K^{15}NO_3$. The ^1H NMR spectra of the electrolyte after electrocatalytic reduction of $K^{15}NO_3$ showed the typical double peaks of $^{15}NH_4^+$ at chemical displacements of 6.75 and 7.0 ppm (Figure 4B(b), curve orange), which further confirms that the formation of ammonia is originated from the electroreduction of $K^{15}NO_3$. Also, the solution after electrolysis using $K^{14}NO_3$ was

https://doi.org/10.1021/acssuschemeng.2c06851
ACS Sustainable Chem. Eng. 2023, 11, 6923−6931

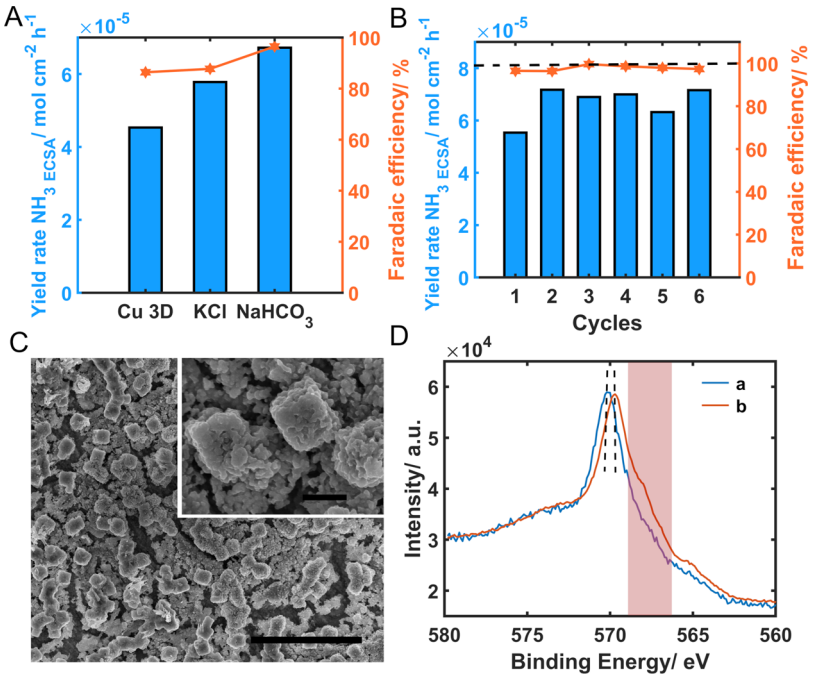

Figure 5. (A) Ammonia YR and FE for the Cu-based 3D-printed electrode after each preparation step: Cu 3D (after bath sonication in HNO_3 1 M), KCl (after KCl treatment), and $NaHCO_3$ (after $NaHCO_3$ treatment). (B) Ammonia YR and FE after each experiment in different electrolytic cycles of 1 h each. (C) The SEM image of the electrode after 1 h of electrolysis in KOH 1 M + KNO_3 0.1 M (black bar = 5 μm). The inset represents a detailed image with a higher magnification (black bar = 500 nm). (D) Comparison of detailed XPS Cu LMM spectra for the initial Cu 3D $NaHCO_3$-treated electrode (a, blue) and after 1 h of electrolysis (b, orange).

evaluated, demonstrating that only $^{14}NH_4^+$ is present (Figure 4B(a), curve blue). This is an extra demonstration of the origin of ammonia from nitrate. In addition, ^{1}H NMR spectra also served to double-check the accuracy of the colorimetric method by considering that the peak area of ^{1}H NMR was related to the ammonia content, and the concentration of ammonium was further quantified by ^{1}H NMR (see Figure S12). Figure 4C,D shows a similar value of ammonia obtained after an electrolytic experiment by using the indophenol blue colorimetric method (62.06 μM (166 ppm) dilution 1:50, R^2 = 0.9999) and ^{1}H NMR method (58.71 μM (157 ppm), R^2 = 0.9992), respectively. As can be observed, the two ammonia content as determined by the two different methods yields a similar ammonia content (green symbol in both calibration curves), providing additional confirmation of the accuracy of the colorimetric method used for ammonia quantification.

Based on the previous results, −0.92 V was chosen as the operating voltage to evaluate catalyst performance and stability. Figure 5A depicts the FE and YR for 3D-printed, KCl-treated Cu and $NaHCO_3$-treated Cu electrodes. As can be observed, the $NaHCO_3$-treated Cu 3D electrode is the most active, not only in terms of FE but also in YR, confirming that the modification of the electrode is highly effective for improving the performance of copper-based 3D-printed electrodes. The stability of the electrocatalyst is paramount for future applications in electrolyzers. Assessment of the stability and durability of the catalyst has been carried out by performing consecutive electrolytic cycles, so that the efficiency and performance of the electrocatalyst can be monitored for a reasonable time frame, with the extrapolation of the performance to longer time periods being possible. For this purpose, six electrolytic cycles of one hour each were performed, refreshing the solution between cycles, and conserving the resulting electrolyte for further analysis of the ammonia content. Results are displayed in Figure 5B, in which the FE, between 96.5 and 99.6%, and YR for ammonia, between 5.5 × 10^{-5} and 7.2 × 10^{-5} mol cm^{-2} h^{-1}, remain stable in different cycles of electrolysis and show no obvious decay over the cycles. In fact, after several electrolytic cycles, the net FE value seems to increase, which is an unexpected result considering most of the reported data on the stability of electrocatalysts. This is very interesting for real applications since repeated cycling does not lead to a severe deactivation of the electrode in terms of both FE and YR. Interestingly, some morphological changes after several cycles of use were observed. The faceted surface was converted into a more aggregated and particulate surface that seems to increase the specific surface area (Figure 5C) as has been demonstrated in some recent works.[25,29] This morphological change involves an apparent increase in roughness with a resulting cauliflower-like surface on the cubes. To further evaluate whether there is an effective increase in the specific area, the ECSA was measured before and after the six electrolytic cycles. Results for the measured area are shown in Table S4. From the values shown in the table, an increase of about 3 times in the ECSA was achieved after the stability test experiment. On the other hand, high-resolution Cu LMM spectra for the electrode before and after the electrolysis (1 h) shows signals corresponding to the composition mainly of Cu^+ as confirmed with the presence of the peak at 932.3 eV for Cu 2p and 570 eV in the Cu LMM region (Figure 5D). Additionally, there is a difference of 0.3 eV (dashed curves) between the two electrodes, before (a, blue) and after electrolysis (b, orange). As can be observed, the region around 568 eV presents a shoulder in the case of the electrode after 1 h electrolysis (orange box). These two observations can confirm that the electrode has more composition of Cu^0 after the electrolysis (Figure S13), which on the one hand is expected due to the cathodic potentials

https://doi.org/10.1021/acssuschemeng.2c06851
ACS Sustainable Chem. Eng. 2023, 11, 6923−6931

applied, and, on the other hand, agrees with a previous report in which the authors claim that the active material is the Cu/Cu_2O resulting from the evolution of the initial electrode (CuO).[13] Therefore, the resulting electrode after the electrolysis is mainly composed of Cu_2O with more composition of Cu^0 compared with the initial electrode, this suggests that the active material for efficient NRA is the partially reduced Cu_2O electrode or Cu/Cu_2O.

Based on the previous data from SEM images and XPS analysis, the change in morphology and composition does not harm the performance of the electrode in terms of FE and YR for ammonia. Additionally, the composition of the electrode to be mainly Cu/Cu_2O, makes this prepared $NaHCO_3$-treated Cu 3D electrode an ideal candidate to be incorporated in electrolyzers, not only because of the high FE obtained but also, and more importantly, because of the remarkable stability in time, with even a slight improvement in efficiency with the number of electrolytic cycles.

CONCLUSIONS

Point-of-use mass production 3D printing technique was used to fabricate copper-based electrodes. $NaHCO_3$-treated Cu 3D-printed nanostructured electrodes exhibited excellent FE, selectivity, and YR for electrocatalytic NRA, reaching a maximum of 96.5% (FE), 95% (selectivity), and 6.72×10^{-5} mol cm^{-2} h^{-1} (YR_{ECSA}) at −0.92 V as the optimum potential. The origin of the nitrogen source for the ammonia produced in the NRA was confirmed by ^{15}N isotope labeling experiments. High stability and durability of the Cu-based 3D-printed electrodes were demonstrated by obtaining a stable or slight increase of the value for FE after several successive electrolytic cycle experiments. The combination of SEM, XPS, and XRD characterization revealed that the presence of Cu/Cu_2O on the electrode surface with cubic facets is the main responsible for the high FE, selectivity, and YR achieved. Cu-based 3D-printed electrodes have been used for nitrate reduction to ammonia for the first time, paving the way for the development of future scalable, point-of-use fabricated, and efficient electrodes for nitrate reduction to ammonia.

ASSOCIATED CONTENT

Supporting Information

The Supporting Information is available free of charge at https://pubs.acs.org/doi/10.1021/acssuschemeng.2c06851.

XPS deconvolutions for Cu 2p and Cu LMM spectra; XPS survey spectra; SEM images; ECSA calculation; tables with compositions by XPS and tables for ECSA values; colorimetric calibration curves for ammonia, nitrite, and nitrate; and ^1H NMR ammonia calibration experiment (PDF)

AUTHOR INFORMATION

Corresponding Author

Martin Pumera − *Future Energy and Innovation Laboratory, Central European Institute of Technology, Brno University of Technology, 61200 Brno, Czech Republic; Faculty of Electrical Engineering and Computer Science, VSB - Technical University of Ostrava, 70800 Ostrava, Czech Republic; Department of Chemical and Biomolecular Engineering, Yonsei University, Seoul 03722, Korea; Department of Medical Research, China Medical University Hospital, China Medical University, Taichung 404, Taiwan;* orcid.org/0000-0001-5846-2951; Email: pumera.research@gmail.com

Authors

Juan V. Perales-Rondon − *Future Energy and Innovation Laboratory, Central European Institute of Technology, Brno University of Technology, 61200 Brno, Czech Republic;* orcid.org/0000-0001-7182-6289

Daniel Rojas − *Future Energy and Innovation Laboratory, Central European Institute of Technology, Brno University of Technology, 61200 Brno, Czech Republic*

Wanli Gao − *Future Energy and Innovation Laboratory, Central European Institute of Technology, Brno University of Technology, 61200 Brno, Czech Republic*

Complete contact information is available at: https://pubs.acs.org/10.1021/acssuschemeng.2c06851

Notes

The authors declare no competing financial interest.

ACKNOWLEDGMENTS

M.P. acknowledges the financial support of the Grant Agency of the Czech Republic (EXPRO: 19-26896X).

REFERENCES

(1) Erisman, J. W.; Sutton, M. A.; Galloway, J.; Klimont, Z.; Winiwarter, W. How a Century of Ammonia Synthesis Changed the World. *Nat. Geosci.* **2008**, *1*, 636−639.

(2) Smil, V. Detonator of the Population Explosion. *Nature* **1999**, *400*, 415.

(3) van Langevelde, P. H.; Katsounaros, I.; Koper, M. T. M. Electrocatalytic Nitrate Reduction for Sustainable Ammonia Production. *Joule* **2021**, *5*, 290−294.

(4) Lim, J.; Fernández, C. A.; Lee, S. W.; Hatzell, M. C. Ammonia and Nitric Acid Demands for Fertilizer Use in 2050. *ACS Energy Lett.* **2021**, *6*, 3676−3685.

(5) MacFarlane, D. R.; Cherepanov, P. V.; Choi, J.; Suryanto, B. H. R.; Hodgetts, R. Y.; Bakker, J. M.; Ferrero Vallana, F. M.; Simonov, A. N. A Roadmap to the Ammonia Economy. *Joule* **2020**, *4*, 1186−1205.

(6) Smith, C.; Hill, A. K.; Torrente-Murciano, L. Current and Future Role of Haber−Bosch Ammonia in a Carbon-Free Energy Landscape. *Energy Environ. Sci.* **2020**, *13*, 331−344.

(7) Foster, S. L.; Bakovic, S. I. P.; Duda, R. D.; Maheshwari, S.; Milton, R. D.; Minteer, S. D.; Janik, M. J.; Renner, J. N.; Greenlee, L. F. Catalysts for Nitrogen Reduction to Ammonia. *Nat. Catal.* **2018**, *1*, 490−500.

(8) Liu, A.; Yang, Y.; Ren, X.; Zhao, Q.; Gao, M.; Guan, W.; Meng, F.; Gao, L.; Yang, Q.; Liang, X.; Ma, T. Current Progress of Electrocatalysts for Ammonia Synthesis Through Electrochemical Nitrogen Reduction Under Ambient Conditions. *ChemSusChem* **2020**, *13*, 3766−3788.

(9) Shahid, U. B.; Siddharth, K.; Shao, M. Electrifying the Nitrogen Cycle: An Electrochemical Endeavor. *Curr. Opin. Electrochem.* **2021**, *30*, No. 100790.

(10) McEnaney, J. M.; Blair, S. J.; Nielander, A. C.; Schwalbe, J. A.; Koshy, D. M.; Cargnello, M.; Jaramillo, T. F. Electrolyte Engineering for Efficient Electrochemical Nitrate Reduction to Ammonia on a Titanium Electrode. *ACS Sustainable Chem. Eng.* **2020**, *8*, 2672−2681.

(11) Daiyan, R.; Tran-Phu, T.; Kumar, P.; Iputera, K.; Tong, Z.; Leverett, J.; Khan, M. H. A.; Esmailpour, A. A.; Jalili, A.; Lim, M.; et al. Nitrate Reduction to Ammonium: From CuO Defect Engineering to Waste NOx-to-NH3 Economic Feasibility. *Energy Environ. Sci.* **2021**, *14*, 3588−3598.

(12) Wang, Y.; Wang, C.; Li, M.; Yu, Y.; Zhang, B. Nitrate Electroreduction: Mechanism Insight,: In Situ Characterization,

Performance Evaluation, and Challenges. *Chem. Soc. Rev.* **2021**, *50*, 6720−6733.
(13) Wang, Y.; Zhou, W.; Jia, R.; Yu, Y.; Zhang, B. Unveiling the Activity Origin of a Copper-Based Electrocatalyst for Selective Nitrate Reduction to Ammonia. *Angew. Chem., Int. Ed.* **2020**, *59*, 5350−5354.
(14) Hu, Q.; Qin, Y.; Wang, X.; Wang, Z.; Huang, X.; Zheng, H.; Gao, K.; Yang, H.; Zhang, P.; Shao, M.; He, C. Reaction Intermediate-Mediated Electrocatalyst Synthesis Favors Specified Facet and Defect Exposure for Efficient Nitrate-Ammonia Conversion. *Energy Environ. Sci.* **2021**, *14*, 4989−4997.
(15) Stefano, J. S.; Kalinke, C.; Da Rocha, R. G.; Rocha, D. P.; Da Silva, V. A. O. P.; Bonacin, J. A.; Angnes, L.; Richter, E. M.; Janegitz, B. C.; Muñoz, R. A. A. Electrochemical (Bio)Sensors Enabled by Fused Deposition Modeling-Based 3D Printing: A Guide to Selecting Designs, Printing Parameters, and Post-Treatment Protocols. *Anal. Chem.* **2022**, *94*, 6417−6429.
(16) Browne, M. P.; Redondo, E.; Pumera, M. 3D Printing for Electrochemical Energy Applications. *Chem. Rev.* **2020**, *120*, 2783−2810.
(17) Rocha, D. P.; Rocha, R. G.; Castro, S. V.; Trindade, M. A.; Munoz, R. A.; Richter, E. M.; Angnes, L. Posttreatment of 3D-printed Surfaces for Electrochemical Applications: A Critical Review on Proposed Protocols. *Electrochem. Sci. Adv.* **2021**, *2*, No. e2100136.
(18) Redondo, E.; Muñoz, J.; Pumera, M. Green Activation Using Reducing Agents of Carbon-Based 3D Printed Electrodes: Turning Good Electrodes to Great. *Carbon* **2021**, *175*, 413−419.
(19) Nyamekye, P.; Nieminen, P.; Bilesan, M. R.; Repo, E.; Piili, H.; Salminen, A. Prospects for Laser Based Powder Bed Fusion in the Manufacturing of Metal Electrodes: A Review. *Appl. Mater. Today* **2021**, *23*, No. 101040.
(20) Ambrosi, A.; Moo, J. G. S.; Pumera, M. Helical 3D-Printed Metal Electrodes as Custom-Shaped 3D Platform for Electrochemical Devices. *Adv. Funct. Mater.* **2016**, *26*, 698−703.
(21) Muñoz, J.; Iffelsberger, C.; Redondo, E.; Pumera, M. Design of Bimetallic 3D-Printed Electrocatalysts via Galvanic Replacement to Enhance Energy Conversion Systems. *Appl. Catal., B* **2022**, *316*, No. 121609.
(22) Wang, Y.; Yu, Y.; Jia, R.; Zhang, C.; Zhang, B. Electrochemical Synthesis of Nitric Acid from Air and Ammonia through Waste Utilization. *Natl. Sci. Rev.* **2019**, *6*, 730−738.
(23) Wu, Z. Y.; Karamad, M.; Yong, X.; Huang, Q.; Cullen, D. A.; Zhu, P.; Xia, C.; Xiao, Q.; Shakouri, M.; Chen, F. Y.; et al. Electrochemical Ammonia Synthesis via Nitrate Reduction on Fe Single Atom Catalyst. *Nat. Commun.* **2021**, *12*, No. 2870.
(24) Kim, T.; Palmore, G. T. R. A Scalable Method for Preparing Cu Electrocatalysts That Convert CO2 into C2 + Products. *Nat. Commun.* **2020**, *11*, No. 3622.
(25) Arán-Ais, R. M.; Rizo, R.; Grosse, P.; Algara-Siller, G.; Dembélé, K.; Plodinec, M.; Lunkenbein, T.; Chee, S. W.; Roldan Cuenya, B. Imaging Electrochemically Synthesized Cu2O Cubes and Their Morphological Evolution under Conditions Relevant to CO2 Electroreduction. *Nat. Commun.* **2020**, *11*, No. 3489.
(26) Siegfried, M. J.; Choi, K. S. Electrochemical Crystallization of Cuprous Oxide with Systematic Shape Evolution. *Adv. Mater.* **2004**, *16*, 1743−1746.
(27) Gao, D.; Zegkinoglou, I.; Divins, N. J.; Scholten, F.; Sinev, I.; Grosse, P.; Roldan Cuenya, B. Plasma-Activated Copper Nanocube Catalysts for Efficient Carbon Dioxide Electroreduction to Hydrocarbons and Alcohols. *ACS Nano* **2017**, *11*, 4825−4831.
(28) Bae, S. E.; Stewart, K. L.; Gewirth, A. A. Nitrate Adsorption and Reduction on Cu(100) in Acidic Solution. *J. Am. Chem. Soc.* **2007**, *129*, 10171−10180.
(29) Grosse, P.; Yoon, A.; Rettenmaier, C.; Herzog, A.; Chee, S. W.; Roldan Cuenya, B. Dynamic Transformation of Cubic Copper Catalysts during CO2 Electroreduction and Its Impact on Catalytic Selectivity. *Nat. Commun.* **2021**, *12*, No. 6736.

https://doi.org/10.1021/acssuschemeng.2c06851
ACS Sustainable Chem. Eng. 2023, 11, 6923−6931